Journal of Solid State Chemistry 183 (2010) 2644–2649

Contents lists available at ScienceDirect

Journal of Solid State Chemistry

journal homepage: www.elsevier.com/locate/jssc

Hydrazine-hydrothermal method to synthesize three-dimensional chalcogenide framework for photocatalytic hydrogen generation

Yi Liu [a], Pushkar D. Kanhere [a], Chui Ling Wong [a], Yuefeng Tian [b], Yuhua Feng [c], Freddy Boey [a], Tom Wu [b], Hongyu Chen [c], Tim J. White [a], Zhong Chen [a], Qichun Zhang [a,*]

[a] School of Materials Science and Engineering, Nanyang Technological University, Singapore 639798, Singapore
[b] Division of Physics and Applied Physics, School of Physical and Mathematical Sciences, Nanyang Technological University, Singapore 637371, Singapore
[c] Department of Chemistry and Biological Chemistry, Nanyang Technological University, Singapore 639798, Singapore

ARTICLE INFO

Article history:
Received 17 July 2010
Received in revised form
9 September 2010
Accepted 12 September 2010
Available online 17 September 2010

Keywords:
Chalcogenide materials
Crystal structure
Optical
Magnetic
Photocatalytic

ABSTRACT

A novel chalcogenide, $[Mn_2Sb_2S_5(N_2H_4)_3]$ (1), has been synthesized by the hydrazine-hydrothermal method. X-ray crystallography study reveals that the new compound **1** crystallizes in space group $P\bar{1}$ (no. 2) of the triclinic system. The structure features an open neutral three-dimensional framework, where two-dimensional mesh-like inorganic layers are bridged by intra- and inter-layer hydrazine ligands. Both two Mn1 and Mn2 sites adopt distorted octahedral coordination. While two Sb1 and Sb2 sites exhibit two different coordination geometries, the Sb1 site is coordinated with three S atoms to generate a SbS_3 trigonal-pyramidal geometry, and the Sb2 site adopts a SbS_4 trigonal bipyramidal coordination geometry. It has an optical band gap of about ~2.09 eV, which was deduced from the diffuse reflectance spectrum, and displays photocatalytic behaviors under visible light irradiation. Magnetic susceptibility measurements show compound **1** obeys the Curie–Weiss law in the range of 50–300 K.

1. Introduction

Crystalline chalcogenide materials not only have fundamental interests in their diverse structures but also pose significant synthetic challenges and display unique structure–property correlations [1–3]. The potential applications of chalcogenide materials can be found in superconductors [4], field-effect transistors [5], visible-light photocatalysts [6], gas separators [7], nonlinear optical generators [8], photoluminescence [9], photoconductors [10], thermoelectrics [11], ion exchangers [12], fast ion conductors [13], porous materials [14], and magnetism [15]. In particular, a broad range of chalcogenide-based semiconducting materials is being considered for solar energy conversion due to current energy problems. It is believed that high crystallinity and large surface area are two basic requirements for enhanced visible-light-driven photocatalytic activities. At the same time, an appropriate narrow band gap (around 2.0 eV) with the right positions of bands is also very important for photocatalysis. Therefore, finding a good synthetic condition to satisfy the above requirements is a big challenge.

Among the various synthetic methods to prepare chalcogenides [16–23], the solvo(hydro)thermal method has proved to be an efficient way of producing crystalline porous chalcogenide frameworks. In particular, hydrazine is a basic solvent with strong coordination and reduction ability. The use of hydrazine in solvo(hydro)thermal synthesis could be promising to produce novel porous crystalline chalcogenide materials [24–27]. Here, we report the synthesis, structural characterization, optical property, magnetic property, and visible-light photocatalytic behavior of a new three-dimensional neutral hydrazine-bridged chalcogenide framework $[Mn_2Sb_2S_5(N_2H_4)_3]$ (**1**). Note that it is first time that metal-hydrazine chalcogenide chemistry is extended towards Mn/pnictide-hydrazine chalcogenides.

2. Experimental section

2.1. Materials and general methods

All reagents were purchased commercially and used without further purification. Elemental analyses (N, H and S) were performed on a Perkin-Elmer 2400 CHN Elemental Analyzer. The elemental analyses of Mn, Sb and S have been examined with the aid of an EDX-equipped JEOL/JSM-6360A SEM. The IR spectrum was obtained on a Perkin-Elmer FT-IR spectrophotometer in the 500–4000 cm^{-1} region with a KBr pellet. Thermal stability studies were carried out on a TGA Q500 instrument under N_2 at a heating

* Corresponding author.
E-mail address: qczhang@ntu.edu.sg (Q. Zhang).

0022-4596/$ - see front matter © 2010 Elsevier Inc. All rights reserved.
doi:10.1016/j.jssc.2010.09.013

rate of 10 °C/min. Powder X-ray diffraction data were recorded on a Bruker D8 Advance diffractometer with a graphite-monochromatized Cu$K\alpha$ radiation. The operating 2θ angle ranges from 10° to 65°. The DC magnetic susceptibility measurements were made on an MPMS magnetometer at temperatures between 5.0 and 300 K.

2.2. Synthesis

A mixture of Mn (1.0 mmol, 0.055 g), Sb_2S_3 (0.4 mmol, 0.136 g), S (1.0 mmol, 0.032 g), and hydrazine monohydrate (4 mL, 98%) was mixed in a 23 mL Teflon-lined stainless steel autoclave. (*Note: More attention should be paid due to hydrazine monohydrate toxicity and strongly reducing ability.*) The autoclave was sealed and heated at 140 °C for 7 days without any disturbance. Then, the autoclave was taken out and cooled to room temperature at its natural cooling rate. The dark-red crystals **1** were isolated in 70% yield (based on Sb_2S_3), washed several times with deionized water, acetone, and ethanol, and air-dried. The crystals appear to be stable in air for months. Anal. calc. for $Mn_2Sb_2S_5N_6H_{12}$ **1**: H, 1.99%; N, 13.83%; S, 26.31% (calculated). Found: H, 2.13%; N, 14.05%; S, 26.85% (experimental). EDS analysis of Mn/Sb/S ratio in **1**: 1:1:2.4.

2.3. Single-crystal structure determination

A dark-red block of crystal of $0.25 \times 0.20 \times 0.12$ mm^3 from reaction **1** was mounted on a glass fiber. Single crystal X-ray diffraction data were collected on a Bruker APEX II CCD diffractometer equipped with a graphite-monochromatized Mo$K\alpha$ radiation source ($\lambda = 0.71073$ Å) at 293 K. Empirical absorption was performed, and the structure was solved by direct methods and refined with the aid of a SHELX-TL program package. All hydrogen atoms were calculated and refined using a riding model. The anisotropic refinement converged to $R_1 = 0.0693$, $wR_2 = 0.2256$ for $I > 2\sigma(I)$ data. Because of the disorder of the free N_2H_4 molecules, it was impossible to locate them in the final structural refinement and this can account for the relatively high R_1 value. Crystallographic data and structural refinements are summarized in Table 1. Atomic positions and anisotropic displacement parameters are provided in Table 2. Selected bond lengths and angles are listed in Table 3. Crystallographic data have been deposited with the Cambridge Crystallographic Data Center as supplementary publication no. 779023. Copy of this data can be obtained free of charge from The Cambridge Crystallographic Data Center via www.ccdc.cam.ac.uk/datarequest/cif.

Table 1
Crystallographic data for $Mn_2Sb_2S_5(N_2H_4)_3$.

Empirical formula	$Mn_2Sb_2S_5(N_2H_4)_3$
Formula weight	609.78
Crystal system	Triclinic
Space group	$P\bar{1}$ (no. 2)
a (Å)	8.814(2)
b (Å)	8.858(2)
c (Å)	8.947(2)
α (deg.)	70.04(3)
β (deg.)	85.98(3)
γ (deg.)	64.07(3)
V (Å^3)	587.9(2)
Z	2
D_{cal} (g/cm^3)	3.264
μ (mm^{-1})	7.493
GOF	1.173
R_1[a]	0.0693
wR_2[b]	0.2256

[a] $R_1 = \Sigma||F_o| - |F_c||/\Sigma|F_o|$.
[b] $wR_2 = [\Sigma w(F_o^2 - F_c^2)^2/\Sigma w(F_o^2)^2]^{1/2}$.

Table 2
Atomic positions and equivalent isotropic displacement parameters for $Mn_2Sb_2S_5(N_2H_4)_3$.

Atom	x	y	z	U_{eq} (Å^2)[a]
Sb(1)	0.82148(17)	0.76464(18)	0.30025(16)	0.0145(5)
Sb(2)	1.34105(17)	1.00431(18)	0.15462(16)	0.0138(5)
Mn(1)	0.8799(4)	1.1962(4)	0.0485(4)	0.0163(7)
Mn(2)	0.5455(4)	1.1831(4)	0.4089(4)	0.0162(8)
S(1)	0.8910(7)	0.6845(7)	0.0600(6)	0.0180(11)
S(2)	0.5838(7)	0.6847(7)	0.3626(6)	0.0166(11)
S(3)	0.6598(6)	1.0850(7)	0.1685(6)	0.0136(11)
S(4)	1.1253(7)	0.8921(7)	0.2030(6)	0.0157(11)
S(5)	1.2814(7)	1.1266(7)	0.3726(6)	0.0152(11)
N(1)	0.687(3)	1.493(2)	−0.096(2)	0.026(4)
N(2)	0.801(2)	1.210(3)	0.399(2)	0.022(4)
N(3)	0.402(2)	1.466(2)	0.246(2)	0.021(4)
N(4)	0.856(2)	1.303(2)	0.256(2)	0.019(4)

[a] U_{eq} is defined as one-third of the trace of the orthogonalized U_{ij} tensor.

Table 3
Bond lengths (Å) and angles (deg.) for $Mn_2Sb_2S_5(N_2H_4)_3$.

Sb(1)–S(3)	2.427(6)	Mn(1)–S(4)#1	2.632(6)
Sb(1)–S(1)	2.445(5)	Mn(1)–S(1)#1	2.651(6)
Sb(1)–S(2)	2.463(5)	Mn(2)–N(3)	2.235(17)
Sb(2)–S(4)	2.457(5)	Mn(2)–N(2)	2.357(18)
Sb(2)–S(5)	2.461(5)	Mn(2)–S(3)	2.569(6)
Sb(2)–S(1)#1	2.734(6)	Mn(2)–S(5)#3	2.602(6)
Sb(2)–S(2)#2	2.778(6)	Mn(2)–S(2)#4	2.644(6)
Mn(1)–N(4)	2.310(19)	Mn(2)–S(5)#5	2.648(6)
Mn(1)–N(1)	2.357(19)	N(1)–N(3)#6	1.46(3)
Mn(1)–S(3)	2.558(6)	N(2)–N(4)	1.45(3)
Mn(1)–S(4)	2.574(6)	N(4)–Mn(1)–S(1)#1	88.8(5)
S(3)–Sb(1)–S(1)	97.60(18)	N(1)–Mn(1)–S(1)#1	83.2(5)
S(3)–Sb(1)–S(2)	98.62(18)	S(3)–Mn(1)–S(1)#1	176.6(2)
S(1)–Sb(1)–S(2)	97.60(18)	S(4)–Mn(1)–S(1)#1	88.0(2)
S(4)–Sb(2)–S(5)	96.49(18)	S(4)#1–Mn(1)–S(1)#1	92.58(19)
S(4)–Sb(2)–S(1)#1	88.57(17)	N(3)–Mn(2)–N(2)	92.2(7)
S(5)–Sb(2)–S(1)#1	93.14(17)	N(3)–Mn(2)–S(3)	90.6(5)
S(4)–Sb(2)–S(2)#2	92.16(17)	N(2)–Mn(2)–S(3)	80.5(5)
S(5)–Sb(2)–S(2)#2	88.92(17)	N(3)–Mn(2)–S(5)#3	171.7(5)
S(1)#1–Sb(2)–S(2)#2	177.72(16)	N(2)–Mn(2)–S(5)#3	84.3(5)
N(4)–Mn(1)–N(1)	84.3(7)	S(3)–Mn(2)–S(5)#3	96.25(19)
N(4)–Mn(1)–S(3)	87.8(5)	N(3)–Mn(2)–S(2)#4	84.1(5)
N(1)–Mn(1)–S(3)	97.0(5)	N(2)–Mn(2)–S(2)#4	99.0(5)
N(4)–Mn(1)–S(4)	92.9(5)	S(3)–Mn(2)–S(2)#4	174.6(2)
N(1)–Mn(1)–S(4)	170.8(5)	S(5)#3–Mn(2)–S(2)#4	88.98(19)
S(3)–Mn(1)–S(4)	91.6(2)	N(3)–Mn(2)–S(5)#5	88.8(5)
N(4)–Mn(1)–S(4)#1	173.4(5)	N(2)–Mn(2)–S(5)#5	168.3(5)
N(1)–Mn(1)–S(4)#1	89.4(5)	S(3)–Mn(2)–S(5)#5	87.93(18)
S(3)–Mn(1)–S(4)#1	90.86(18)	S(5)#3–Mn(2)–S(5)#5	96.13(19)
S(4)–Mn(1)–S(4)#1	93.65(19)	S(2)#4–Mn(2)–S(5)#5	92.66(19)

Symmetry transformations used to generate equivalent atoms:
#1 $-x+2, -y+2, -z$; #2 $x+1, y, z$; #3 $-x+2, -y+2, -z+1$.
#4 $-x+1, -y+2, -z+1$ #5 $x-1, y, z$ #6 $-x+1, -y+3, -z$.

2.4. Optical properties

The optical diffuse reflectance spectra were measured at room temperature on a Perkin-Elmer Lambda 900 UV–vis-NIR spectrometer equipped with an integrating sphere. $BaSO_4$ was used as the reference material, and the polycrystalline samples were ground well before the measurement. The absorption (α/S) data were calculated from the reflectance using the Kubelka–Munk function: $\alpha/S = (1-R)^2/2R$, in which R is the reflectance at a given wavelength, α is the absorption coefficient, and S is the scattering coefficient [28].

2.5. Magnetic susceptibility

The DC magnetic susceptibility measurements were made on an MPMS magnetometer at temperatures between 5.0 and 300 K. The X-ray pure polycrystalline sample was ground to a fine powder to minimize possible anisotropic effects and loaded into a gelatin capsule. The sample was cooled in a constant magnetic field of 5000 Oe for measurements of magnetization versus temperature. The data were corrected for the susceptibility of the container and for the diamagnetic contribution from the ion core.

2.6. Photocatalysis

The photocatalytic reaction was carried out in a closed-gas circulation system. The reaction cell was made up of Pyrex glass with a quartz window suitable for vertical illumination. A 450 W high pressure Xe lamp (Oriole Instruments, USA) was used as a light source. A 420 nm cut-off filter was employed to screen the UV light. The IR component in the radiation was removed by circulating water filter. The air in the reaction cell was removed by purging the argon gas. In all tests, 100 mg of catalyst was suspended in 100 mL of 0.1 M Na_2S solution by magnetic stirring. The reaction was carried out for 10 h and the amount of hydrogen evolved was analyzed by gas chromatograph (Shimadzu GC-2014; Molecular sieve 5A, TCD detector, Ar carrier gas).

3. Results and discussion

We report here a new three-dimensional neutral hydrazine-bridged chalcogenide framework $[Mn_2Sb_2S_5(N_2H_4)_3]$ (**1**), which was prepared by reacting Mn and Sb_2S_3 with S in N_2H_4/H_2O (1:1) for 4 days at 140 °C. The compound **1** was harvested as dark-red hexagonal crystals (Fig. 1) with 70% yield. The X-ray powder diffraction pattern of **1** agrees with the one simulated from the single-crystal diffraction analysis (Fig. 2). The existence of N_2H_4 molecules was confirmed by IR spectroscopy (Fig. 3) and quantified by elemental and thermogravimetric analysis (TGA, Fig. 4). The calculated Mn/Sb/S atomic ratio from the single-crystal structure analysis is in agreement with energy-dispersive X-ray spectroscopy analysis (EDS, Fig. S1 in the supporting information).

X-ray crystallography study reveals that the new compound **1** crystallizes in the triclinic space group $P\bar{1}$ (no. 2) and features a three-dimensional (3D) framework, where a neutral two-dimensional (2D) net parallel to the *ac* plane is bridged by $H_2N–NH_2$ molecules. The asymmetric unit of **1** contains two crystallographically independent Mn sites, two Sb sites, five S sites, and three $H_2N–NH_2$ neutral molecules (Fig. 5a). Because all three $H_2N–NH_2$ are neutral molecules in compound **1**, the formal oxidation states of Mn/Sb/S can be assigned as 2+/3+/2−, respectively. Both Mn1 and Mn2 sites adopt a distorted octahedral geometry and coordinate with four S atoms and two N atoms located at neighboring vertices of the octahedron coming from two different $H_2N–NH_2$ ligands. Compound **1** has a similar Mn coordination geometry MnS_4N_2 compared to $Mn_2SnS_4(N_2H_4)_2$ [24], while there are two Mn coordination geometries in another

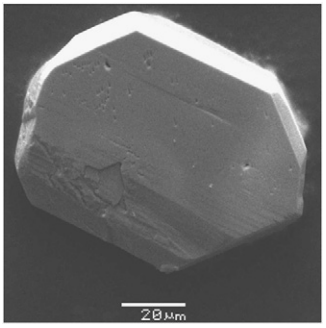

Fig. 1. Scanning secondary electron micrograph image of a typical crystal **1**.

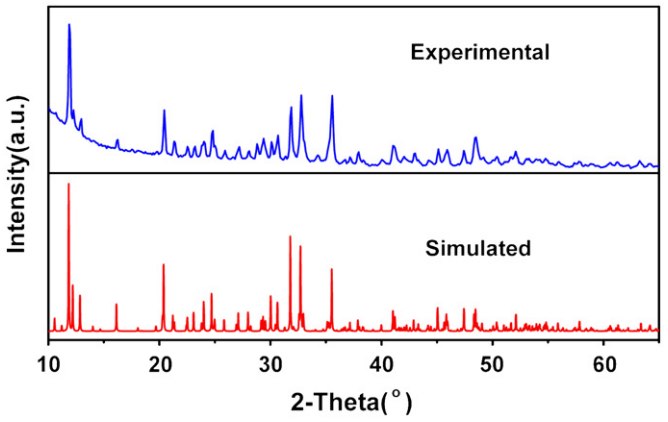

Fig. 2. XRD patterns of compound **1**. Blue: experimental; red: simulation. (For interpretation of the references to colour in this figure legend, the reader is referred to the web version of this article.).

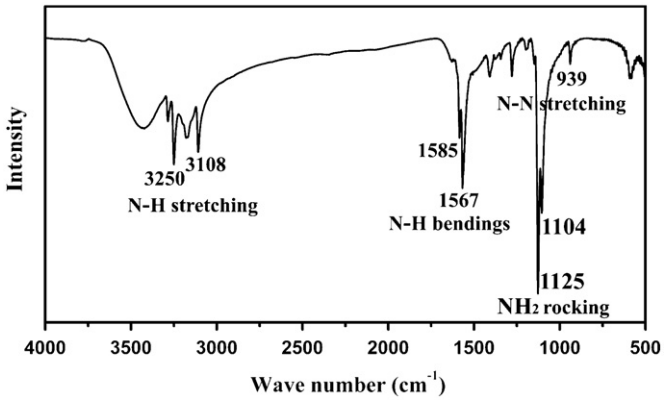

Fig. 3. IR spectrum of compound **1**.

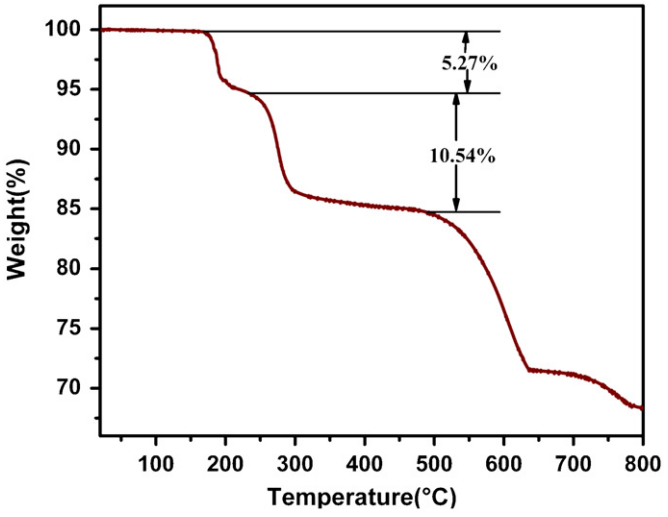

Fig. 4. TGA analysis of compound **1**.

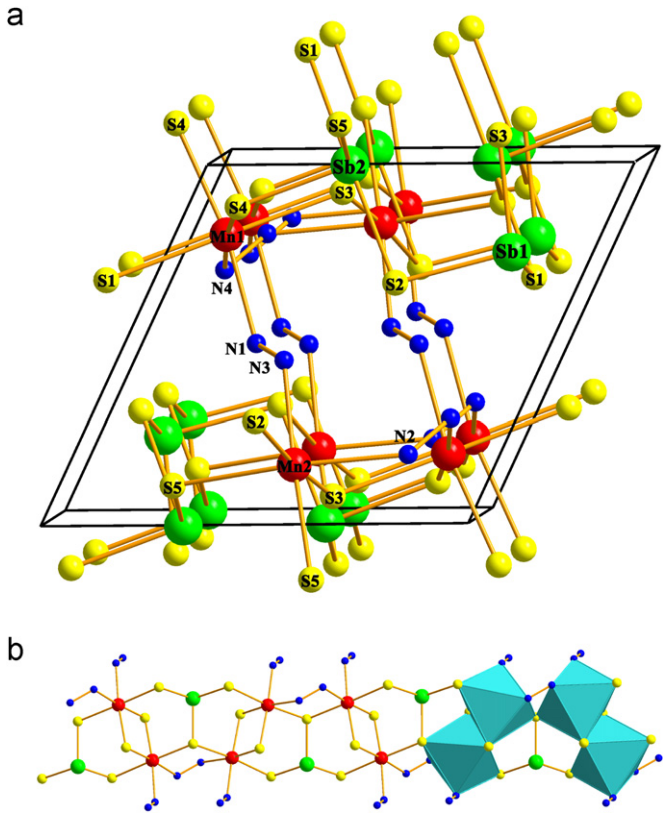

Fig. 5. (a) Ball-stick model of the relevant fragments of compound **1**. (b) Chain in the structure of **1** viewed along the *a* axis. Red, Mn; green, Sb; yellow, S; blue: N. (For interpretation of the references to colour in this figure legend, the reader is referred to the web version of this article.).

reported structure $[Mn(C_6H_{18}N_4)]_4Mn_2Sb_4S_{12}$ [29]: MnN_4S_2 octahedron and MnS_4 tetrahedron. The Mn–S and Mn–N bond distances lie in the ranges of 2.558(6)–2.651(6) and 2.235(17)–2.357(18) Å, respectively. The bond angles of S–Mn–S and N–Mn–S range from 88.0(2)° to 176.6(2)° and from 80.5(5)° to 173.4(5)°, respectively. Interestingly, Sb1 and Sb2 sites exhibit different coordination geometries. The Sb1 site is coordinated with three S atoms to generate a SbS_3 trigonal-pyramidal geometry with Sb–S bond lengths ranging from 2.427(6) to 2.463(5) Å, while the Sb2 site adopts a SbS_4 four-fold coordination geometry with two short (2.457(5) and 2.461(5) Å) and two long (2.734(6) and 2.778(6) Å) Sb–S distances. The bond angles of S–Sb–S range from 88.57(17)° to 177.72(16)°. The similar SbS_4 coordination geometry was also found in $[(Me)_2NH_2]_2[Sb_2GeS_6]$ [30].

It is worth mentioning that **1** has three types of H_2N–NH_2 neutral molecules, which act as three different roles. One type of hydrazine molecules serves as the intra-layer bridged ligands while another type acts as the inter-layer linkers, which is similar to the reported results [24]. The third type occupies in channels and serves as a template for 3D structure. Although the third type of H_2N–NH_2 molecules is disordered and cannot be located from X-ray diffraction, they can be quantified by elemental and thermogravimetric analysis (Fig. 4). In TGA analysis, the first stage (170–220 °C) of weight loss (5.27%) comes from free H_2N–NH_2 molecules (disorder) and the second stage (220–300 °C) of weight loss (10.54%) is from coordinated H_2N–NH_2 molecules. Interestingly, the intra-layer and inter-layer hydrazine coordination modes are also investigated in the structure of $Mn_2SnS_4(N_2H_4)_5$ [27]. But in the structure of $Mn_2SnS_4(N_2H_4)_2$ [24], hydrazine molecules only exist in intra-layer and the layers are connected by Sn–S bonds. Note that no free hydrazine molecules exist in these two structures.

In the 2D layer of **1**, two identical octahedral Mn-centers share one S···S edge to form a $Mn_2S_6N_4$ dimmer, which is further connected by SbS_3 trigonal pyramids and the intra-layer H_2N–NH_2 ligands to form a one-dimensional (1D) linear chain (Fig. 5b). These chains are linked together by four-fold coordinated SbS_4 units via the shared S···S edges to form a layered motif (Fig. 6a). The thickness of Mn/Sb/S/N layer is about 5.6 Å (Fig. 6b). There are two small channels with a size of ~3.8 Å × 5.2 Å and ~8.0 Å × 8.3 Å, perpendicular to the *ac* plane, which are generated by the interconnectivity of the chains. The other two small channels appeared with a rough cross-section of ~3.8 Å × 5.4 Å and ~4.7 Å × 8.2 Å, which are parallel to the *c*-axis. The disordered free H_2N–NH_2 molecules, which cannot be located form X-ray data, might sit in these channels.

Interestingly, Bensch [31] and other groups [32] reported a series of layered thioantimonate (III) frameworks (**2**) with a similar stoichiometry (i.e. $Mn_2Sb_2S_5 \cdot L$ L=2-methylamine [31], ethylenediamine [31], 2-propylamine [31], 1,3-diaminopropane [31], N-methyl-1,3-diaminopropane [31], and phen [32]) to compound **1**. Although $Mn_2Sb_2S_5$ in these compounds form a layer structure, their structural characteristics are totally different. It is worth comparing the structure of compound **1** with that of the related materials **2**. There are several differences between these two structures: (a) **1** is a three-dimensional framework through hydrazine-bridged neighboring $Mn_2Sb_2S_5$ layers while compound **2** is a layer structure; (b) Mn centers in **1** coordinate with two N atoms and four S atoms while **2** has two different

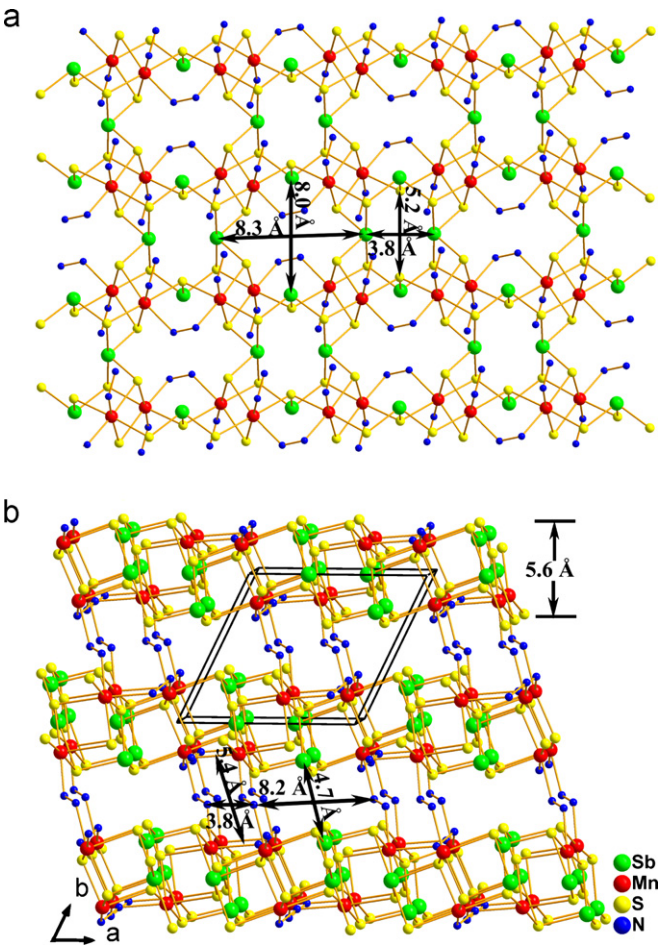

Fig. 6. (a) View of a single layer of compound **1** and (b) view of the three dimensional framework of **1** down the *c*-axis with indication of the pores.

Mn centers: MnS_6 and $Mn_2S_4N_2$; (c) the Sb atoms in **1** has two different coordinations: trigonal pyramids SbS_3 and four-fold coordinated SbS_4 while the configuration of all Sb atoms in **2** is trigonal pyramids SbS_3; and (d) the intra-layer connectivity is different.

The solid state UV–visible absorption for compound **1** revealed an absorption edge at ~2.09 eV, consistent with the red colour (Fig. 7). Infrared spectroscopy (IR, Fig. 3) indicates that there are several peaks between 3250 and 3108 cm^{-1}, which can be assigned to N–H stretching. The peaks at 1585, 1567, 1125, and 1104 cm^{-1} can be assigned to N–H bending (first two) and NH_2 rocking (latter ethics), respectively. In addition, the peak at 939 cm^{-1} is attributed to N–N stretching and is typical for compounds containing bridged H_2N–NH_2 molecules [33].

The magnetic susceptibility for compound **1** (Fig. 8) in the temperature range of 50–300 K was fit by a least-squares method using the Curie–Weiss equation $\chi_M = C/(T-\theta)$, where χ_M is the magnetic susceptibility, C is the Curie constant and θ is the Weiss constant. The effective magnetic moment (μ_{eff}) was calculated from the equation $\mu_{eff} = (7.997C)^{1/2}\,\mu_B$ [34]. The parameters obtained from fitting are as follows: Curie constant, $C = 16.62$ emu K/mol; Weiss temperature, $\theta = -177.57$ K. The negative θ value suggests that there is a significant antiferromagnetic interaction existing between the magnetic Mn ions (the nearest distance between Mn ions is 3.51 Å). The effective magnetic moment (μ_{eff}) for one Mn^{2+} ion in compound **1** is 5.76 μ_B, which is close to a free Mn^{2+} ion (5.92 μ_B) [35].

The photocatalytic reaction showed about 4.64 μmol h^{-1} g^{-1} of H_2 was generated over the $[Mn_2Sb_2S_5(N_2H_4)_3]$ (**1**) catalyst without any co-catalyst under visible light irradiation (Fig. 9). Currently, compound **1** has shown a lower photocatalytic efficiency compared to known inorganic metal sulfide catalysts; however, it is still comparable to that of some organic–inorganic hybrid semiconductors [6a]. Trying to enhance the efficiency of this type of materials through increasing the size of pores is under investigation.

4. Conclusions

In conclusion, a new three-dimensional hydrazine-bridged hybrid metal sulfide framework is described. The $[Mn_2Sb_2S_5(N_2H_4)_3]$ (**1**) has a low electronic band gap of about 2.09 eV and displays visible light photocatalytic activity for hydrogen generation. The magnetic measurement suggests that our material has an antiferromagnetic behavior. Our results have demonstrated that hydrazine/water solvent can provide alternative possibilities to extend metal-hydrazine chalcogenide chemistry towards Mn/pnictide-hydrazine chalcogenides, to which little attention has been paid to so far.

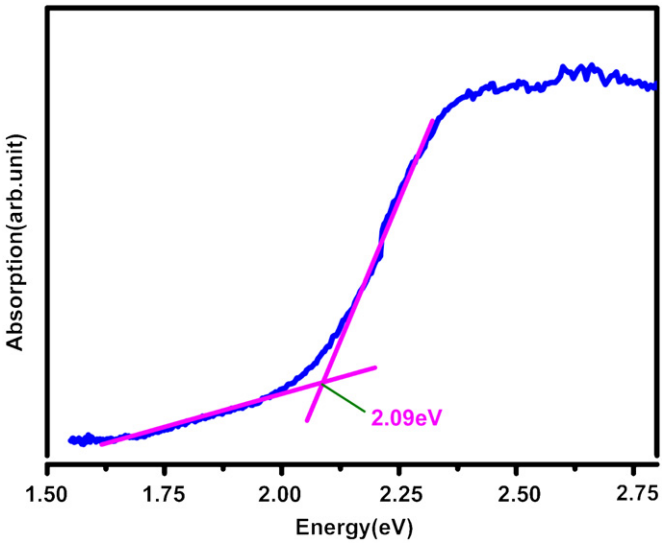

Fig. 7. The UV–visible absorbance of a single crystal of compound **1**.

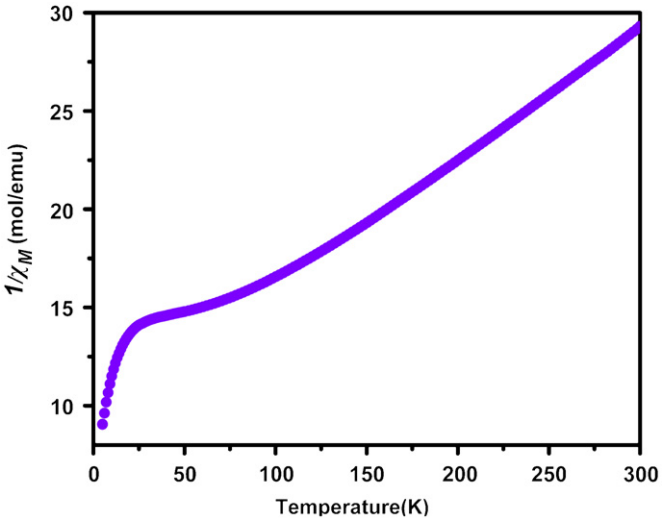

Fig. 8. Plot of $1/\chi_M$ vs. temperature (T) for compound **1**.

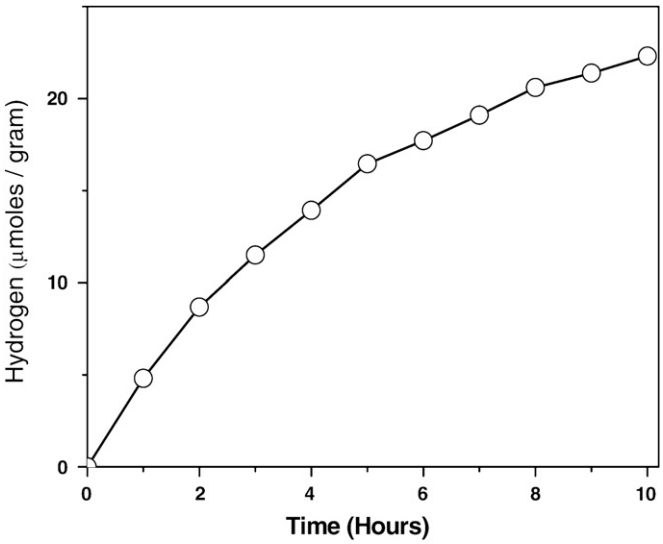

Fig. 9. The photocatalytic hydrogen evolution over sample **1**.

Supporting information available

EDX analysis and X-ray crystallographic data of **1** are available.

Acknowledgment

Financial support from the AcRF Tier 1 (RG 18/09) from MOE is gratefully acknowledged.

Appendix A. Supplementary material

Supplementary data associated with this article can be found in the online version at doi:10.1016/j.jssc.2010.09.013.

References

[1] (a) D.B. Matzi, Adv. Mater. 21 (2009) 314;
(b) J.F. Corrigan, O. Fuhr, D. Fenske, Adv. Mater. 21 (2009) 1867;
(c) M.G. Kanatzidis, K.R. Poeppelmeier, Prog. Solid State Chem. 36 (2008) 1;
(d) S. Dehnen, M. Melullis, Coord. Chem. Rev. 251 (2007) 1259;
(e) P.Y. Feng, X.H. Bu, N.F. Zheng, Acc. Chem. Res. 38 (2005) 293;
(f) M.G. Kanatzidis, Acc. Chem. Res. 38 (2005) 361;
(g) R.L. Bedard, S.T. Wilson, L.D. Vail, J.M. Bennett, E.M. Flanigen, Zeolites: facts, figures, future, in: P.A. Jacobs, R.A. van Santen (Eds.), Proceedings of the 8th International Zeolites Conference, Elsevier, Amsterdam1989, pp. 375–387.

[2] (a) J.B. Parise, Science 251 (1991) 293;
(b) C.L. Cahill, Y. Ko, J.B. Parise, Chem. Mater. 10 (1998) 19;
(c) C.L. Cahill, J.B. Parise, J. Chem. Soc. Dalton Trans. (2000) 1475.

[3] (a) H. Li, A. Laine, M. O'Keeffe, O.M. Yaghi, Science 283 (1999) 1145;
(b) H. Li, M. Eddaoudi, A. Laine, M. O'Keeffe, O.M. Yaghi, J. Am. Chem. Soc. 121 (1990) 6096.

[4] M. Yoshikazu, T. Yoshihiko, Condens. Matter (2010) 1 arXiv.org, e-Print Archive.

[5] J.S. Meth, S.G. Zane, K.G. Sharp, S. Ageawal, Thin Solid Films 444 (2003) 227.

[6] (a) Z.Y. Zhang, J. Zhang, T. Wu, X.H. Bu, P.Y. Feng, J. Am. Chem. Soc. 130 (2008) 15238;
(b) N.F. Zheng, X.H. Bu, H. Vu, P.Y. Feng, Angew. Chem., Int. Ed. 44 (2005) 5299.

[7] G.S. Armatas, M.G. Kanatzidis, Nat. Mater. 8 (2009) 217.

[8] (a) T.K. Bera, J.I. Jang, J.-H. Song, C.D. Malliakas, A.J. Freeman, J.B. Ketterson, M.G. Kanatzidis, J. Am. Chem. Soc. 132 (2010) 3484;
(b) Q.C. Zhang, I. Chung, J.I. Jangg, J.B. Ketterson, M.G. Kanatzidis, J. Am. Chem. Soc. 131 (2009) 9896;
(c) Q.C. Zhang, I. Chung, J.I. Jang, J.B. Ketterson, M.G. Kanatzidis, Chem. Mater. 21 (2009) 12.

[9] (a) M. Wu, T.J. Emge, X.Y. Huang, J. Li, Y. Zhang, J. Solid State Chem. 181 (2008) 415;
(b) Q.C. Zhang, X.H. Bu, L. Han, P.Y. Feng, Inorg. Chem. 45 (2006) 6684.

[10] Q.C. Zhang, Y. Liu, X.H. Bu, T. Wu, P.Y. Feng, Angew. Chem., Int. Ed. 47 (2008) 113.

[11] (a) Y. Lan, A.J. Minnich, G. Chen, Z.F. Ren, Adv. Funct. Mater. 20 (2010) 357;
(b) J.R. Sootsman, D.Y. Chung, M.G. Kanatzidis, Angew. Chem., Int. Ed 48 (2009) 8616;
(c) M.G. Kanatzidis, Chem. Mater. 22 (2010) 648.

[12] (a) M.J. Manos, N. Ding, M.G. Kanatzidis, Proc. Natl. Acad. Sci. USA 105 (2008) 3696;
(b) M.J. Manos, K. Chrissafis, M.G. Kanatzidis, J. Am. Chem. Soc. 128 (2006) 8875.

[13] N.F. Zheng, X.H. Bu, P.Y. Feng, Nature 426 (2003) 428.

[14] (a) S. Bag, P.N. Trikalitis, P.J. Chupas, G.S. Armatas, M.G. Kanatzidis, Science 317 (2007) 490;
(b) N.F. Zheng, X.H. Bu, B. Wang, P.Y. Feng, Science 298 (2002) 2366.

[15] (a) Q.C. Zhang, X.H. Bu, Z.E. Lin, M. Biasini, W.P. Beyemann, P.Y. Feng, Inorg. Chem. 46 (2007) 7262;
(b) J.A. Aitken, J.A. Cowen, M.G. Kanatzidis, Chem. Mater. 10 (1998) 3928.

[16] (a) W.P. Su, X.Y. Huang, J. Li, H.X. Fu, J. Am. Chem. Soc. 124 (2002) 12944;
(b) J. Li, Z. Chen, K.-C. Lam, Inorg. Chem. 36 (1997) 684;
(c) Z. Chen, J. Li, F. Chen, D.M. Proserpio, Inorg. Chem. Acta (1998) 255.

[17] (a) H. Ahari, A. Lough, S. Petrov, G.A. Ozin, R.L. Bedard, J. Mater. Chem. 9 (1999) 1263;
(b) T. Jiang, G.A. Ozin, R.L. Bedard, Adv. Mater. 6 (1994) 860.

[18] (a) E. Ruzin, A. Fuchs, S. Dehnen, Chem. Commun. (2006) 4796;
(b) M. Melullis, R. Clerac, S. Dehnen, Chem. Commun. (2005) 6008;
(c) S. Dehnen, M.K. Brandmayer, J. Am. Chem. Soc. 125 (2003) 6618;
(d) C. Zimmermann, M. Melullis, S. Dehnen, Angew. Chem., Int. Ed. 41 (2002) 4269.

[19] R.C. Burns, J.D. Corbett, Inorg. Chem. 20 (1991) 4433.

[20] (a) C.-C. Wang, R.C. Haushalter, Inorg. Chem. 38 (1999) 595;
(b) S.S. Dhingra, R.C. Haushalter, J. Am. Chem. Soc. 116 (1994) 3651.

[21] S. Dhingra, M.G. Kanatzidis, Science 258 (1992) 1769.

[22] (a) H. Bloom, The Chemistry of Molten Salts, Benjaman, , 1967;
(b) G.J. Janz (Ed.), Molten Salts Handbook, Academic Press, New York, 1967;
(c) G. Mamantov, in: Molten Salts: Characterization and Analysis, Marcel Dekker, New York, 1969;
(d) D. Elwell, H.J. Scheel, in: Crystal Grown from High-Temperature Solutions, Academic Press, London, 1975.

[23] (a) C.-W. Park, R.J. Salm, J.A. Ibers, Angew. Chem. Int. Ed. 34 (1995) 1879;
(b) T.M. Martin, P.T. Wood, J.W. Kolis, Inorg. Chem. 33 (1994) 1587.

[24] M.J. Manos, M.G. Kanatzidis, Inorg. Chem. 48 (2009) 4658.

[25] X.Y. Huang, J. Li, Y. Zhang, A. Mascarenhas, J. Am. Chem. Soc. 125 (2003) 7049.

[26] (a) D.B. Mitzi, Inorg. Chem. 46 (2007) 926;
(b) D.B. Mitzi, Inorg. Chem. 44 (2005) 3755.

[27] M. Yuan, M. Dirmyer, J. Badding, A. Sen, M. Dahlberg, P. Schiffer, Inorg. Chem. 46 (2007) 7238.

[28] G. Kortüm, in: Reflectance Spectroscopy, Springer, New York, 1969.

[29] M. Schaefer, C. Näther, W. Bensch, Solid State Sci. 5 (2003) 1135.

[30] M.L. Feng, D.N. Kong, Z.L. Xie, X.Y. Huang, Angew. Chem. Int. Ed. 47 (2008) 8623.

[31] (a) L. Engelke, M. Schaefer, F. Porsch, W. Bensch, Eur. J. Inorg. Chem. 3 (2003) 506;
(b) L. Engelke, M. Schaefer, M. Schur, W. Bensh, Chem. Mater. 13 (2001) 1383;
(c) M. Schur, C. Nather, W. Bensch, Z. Naturforsch. B 56 (2001) 79;
(d) W. Bensch, M. Schur, Eur. J. Solid. State Inorg. Chem. (1996) 1149.

[32] X. Wang, T.L. Sheng, S.M. Hu, R.B. Fu, X.T. Wu, Inorg. Chem. Commun. 12 (2009) 399.

[33] (a) A. Braibanti, F. Dallavalle, M.A. Pellinghelli, E. Leporati, Inorg. Chem. 7 (1968) 1430;
(b) R. Lascola, R. Withnall, L. Andrews, Inorg. Chem. 27 (1988) 642.

[34] C.J. O'Connor, Prog. Inorg. Chem. 29 (1982) 203.

[35] J.H. Van Vleck, in: The Theory of Electric and Magnetic Susceptibilities, Oxford University, Oxford, UK, 1932.